

THE MAGNETIC FIELD OF HD 215441

GEORGE W. PRESTON

Mount Wilson and Palomar Observatories, Carnegie Institution of Washington,
 California Institute of Technology

Received November 1, 1968

ABSTRACT

Zeeman spectrograms of HD 215441 show evidence for a periodic variation of its magnetic field in 1967. Comparison of intensities and displacements of the Zeeman components resolved on high-dispersion spectrograms with those calculated for inclined dipoles indicate that the magnetic field of HD 215441 is not dipolar. Calculations for other simple, arbitrary geometries suggest the nature of the departures from dipole geometry.

I. INTRODUCTION

The large magnetic field (~ 34 kilogauss) of HD 215441 discovered by Babcock (1960) provides a rare opportunity to study the resolved Zeeman components of a magnetic star and thereby to gain some information about the geometry of the surface magnetic field. If, as Babcock's initial investigation suggested, HD 215441 is an irregular magnetic variable, then it poses a challenge to theories which predict periodic magnetic variations, in particular to the oblique-rotator theory (Stibbs 1950; Deutsch 1954) which has enjoyed some success in explaining the various periodic phenomena of the Ap stars.

In August 1967 a series of Zeeman spectrograms with a dispersion of 8 \AA mm^{-1} of HD 215441 were obtained with the coudé spectrograph of the 120-inch reflector at Lick Observatory in an attempt to find evidence for a periodicity in the effective magnetic field (as derived from unresolved Zeeman patterns). These observations were accompanied by concurrent *UBV* observations by Stepien described elsewhere (Stepien 1968). This reinvestigation was prompted by the suspicion that many of the lines well resolved at 4.5 \AA mm^{-1} (Babcock's higher dispersion) would be marginally resolved at 9 \AA mm^{-1} (Babcock's lower dispersion) and that the irregular variation deduced from the lower-dispersion material was the result of random variations *in the appearance* of these marginally resolved patterns. By taking well-widened (total widening $\sim 0.67 \text{ mm}$) spectrograms and choosing lines with patterns that should not be resolved, I hoped to avoid such difficulties. The above suspicion proved to be correct. In fact, so many profiles are resolved on the 8 \AA mm^{-1} plates that it did not seem feasible to attempt to determine H_e from unresolved patterns in the usual way. Therefore, on the last night of the August run I observed the star at 4 \AA mm^{-1} and obtained three more 4 \AA mm^{-1} spectrograms in October 1967. A journal of the observations is given in Table 1.

II. THE SPECTRUM OF HD 215441

Some sixty resolved Zeeman patterns can be seen on ECZ 5931, portions of which are reproduced in Figures 1*a* and 1*b* (Plates 3 and 4). Most of the patterns are triplets, the strongest component being displaced longward in the upper right-circularly analyzed spectrum, and shortward in the lower, left-circularly analyzed spectrum. However, there are a number of doublet patterns, e.g., lines 12, 23, 42, 52, 58, 67, 77, 88, and 89, and one "quartet" line 83. The numbers identify the lines in Figure 1 and Table 2. The doublet patterns occur in those anomalous Zeeman patterns for which the most displaced π components are the most intense and lie near the most intense σ components. In the case of line 54, Ti II $\lambda 4314.98$, the pattern is (1.33) 1.33; the π and σ components have identi-

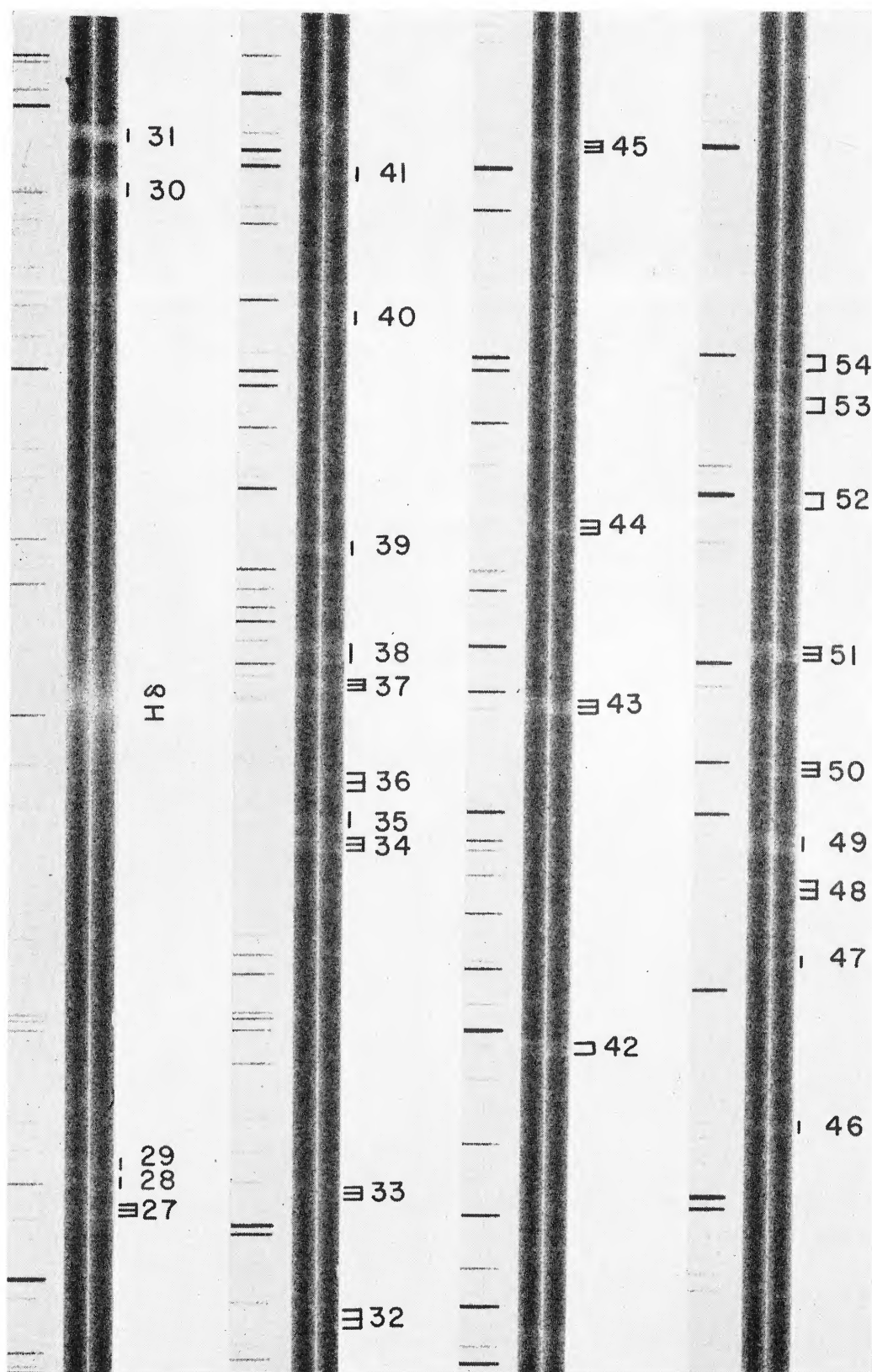


FIG. 1a.—Wavelength region $\lambda\lambda 4065\text{--}4330$ on spectrogram ECZ 5931 of HD 215441. Numbers identify the lines in Table 2. Double and triple markers indicate the doublet and triplet patterns discussed in the text. Horizontal markers denote lines with unresolved Zeeman patterns.

PRESTON (*see page 967*)

PLATE 4

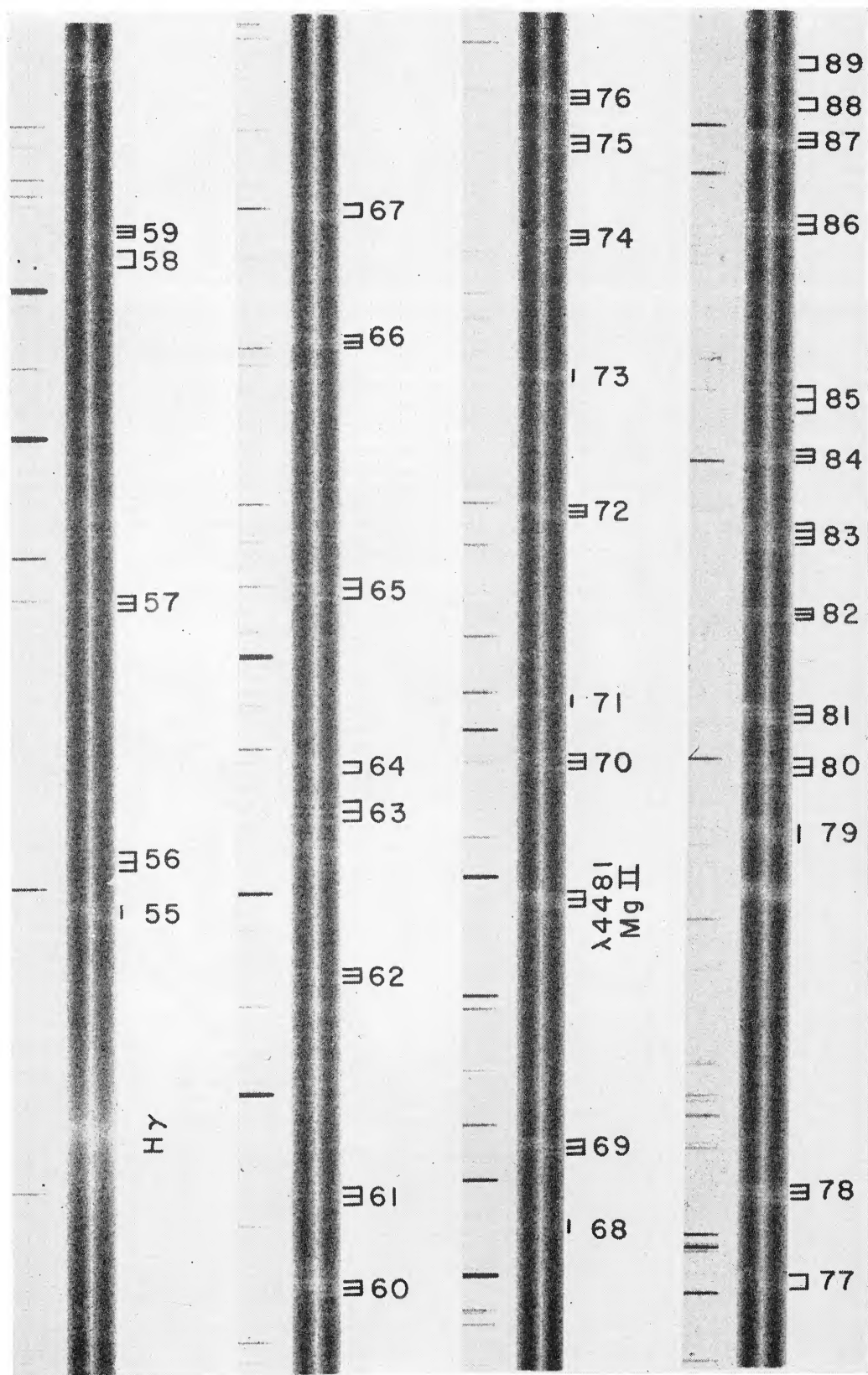


FIG. 1*b*.—Wavelength region $\lambda\lambda 4330\text{--}4595$ on spectrogram ECZ 5931 of HD 215441. The numbering and markers are as in Fig. 1*a*. Note the extremely wide pattern of line 85 and the peculiar structure of line 83, both due to Si III.

PRESTON (*see* page 967)

cal displacements, and the observed doublet components are sharp. For lines 67 and 77 due to $\text{Ti II } \lambda 4450.49$ and $\text{Ti II } \lambda 4529.46$, the patterns are, respectively, (0.17, 0.51, 0.86) 0.34, 0.69, 1.03, 1.37, 1.71 and (0.10, 0.30, 0.50, 0.70, 0.91) 0.20, 0.40, 0.61, 0.81, 1.01, 1.21, 1.41, 1.62, 1.82; the observed doublet components are diffuse, as would be expected from such broad, overlapping π and σ groups. The above patterns and the notation are those of Kiess and Meggers (1928). There are intermediate cases, such as lines 32 and 38, and occasional unusual patterns, such as that for $\text{Ti II } \lambda 44.64.66$, (0.93) 0.13, 1.73. The lone quartet is due to $\text{Si III } \lambda 4567.87$ with the pattern (0.50) 1.50, 2.00; in this case the π group is itself resolved into its two components. The good correspondence between predicted patterns and those observed in HD 215441 indicates the usefulness of LS coupling to predict Zeeman patterns for the elements Si through Fe.

As a preliminary to the study of the magnetic field ECZ 5931, the best of the 4 Å mm^{-1} plates was measured for the purpose of line identification. Approximately 200 features were measured on the interval $\lambda\lambda 3675\text{--}4635$. Ninety-five apparently unblended

TABLE 1
JOURNAL OF OBSERVATIONS

PLATE	DISPERSION (Å mm^{-1})	J D \odot 2439000+	PHASE (eq [2])	H (gauss)		v_{rad} (km sec^{-1})
				8 Å mm^{-1} List	All Lines	
ECZ:						
5837.	8 1	720 893	0 00	35300	.	-6 0
5849..	8 1	721 854	.10	34700	. . .	-5 4
5862.	8 1	722 868	21	33100	. . .	-5 1
5874...	8 1	723 849	.31	32800	. . .	-4 4
5884 .	8 1	724 968	.43	32600	. . .	-5 2
5894..	8 1	725 896	53	31900	. . .	-5 1
5919 .	8 1	728.871	84	34600	-5 3
5931...	4.1	729 892	95	33850	33890	-4 8
6085 .	4 1	775 778	.78	34000	33750	-6 5
6087	4 1	776 737	89	34320	34260	-6 7
6101.	4 1	779 723	0 20	32340	32590	-5 6

lines listed in Table 2 were chosen for measurement of the Zeeman effect. The remaining lines either are blends or could not be identified. The list includes lines of Si II, Si III, Ti II, Cr II, Fe II, Fe III, and Sr II. In addition to lines of H, the spectrum also contains lines of He I and C II. The strong sharp lines of Ca II do not exhibit the Zeeman effect and probably are of interstellar origin.

As Babcock has noted, the very strong magnetic field of HD 215441 is not accompanied by any outstanding peculiarities other than those generally associated with the Ap stars. However, the star appears to be considerably hotter than the Draper type A0p or Osawa's (1965) type B7-B8 would indicate. Cameron (1967) has noted that the Strömgen c_1 index for HD 215441 places it near B3. To this we may add the following estimates: (1) The mean color indices of HD 215441 averaged over the 9^d5 photometric cycle are $\langle B - V \rangle = +0.02$, $\langle U - B \rangle = -0.51$ (Stepien 1968). A reddening line of slope 0.72 intersects Johnson's (1963) unreddened main sequence at $(B - V)_0 = -0.18$, $(U - B)_0 = -0.67$, a fact which also indicates a spectral type near B3 or B4. (2) We estimate that the ratio Si II $\lambda 4130$ /Si III $\lambda 4552$ in HD 215441 is roughly 2 to 3. According to Underhill (1957) such ratios occur near spectral type B4. Thus the Paschen continuum, the Balmer discontinuity, and temperature-sensitive line ratios all indicate a

TABLE 2

LINES IDENTIFIED IN HD 215441

Line No.	λ	El.(RMT) [†]	Z	Zeeman Pattern [‡]	$\Delta\lambda_c$
1	3706.22	Ti II(73)	1.07	(.27, <u>.80</u>) .53, <u>1.07</u> , 1.60	
2	3741.63	Ti II(72)	1.20	(.00) 1.20	
3	3757.68	Ti II(72)	0.80	(.00) .80	
4	3759.29	Ti II(13)	1.14	(.00) 1.14	
5	3761.87	Ti II(107)	1.14	(.00) 1.14	
6	3765.62	Cr II(20)	0.50	(.20) .20, <u>.60</u>	
7	3776.06	Ti II(72)	1.50	(.20, <u>.60</u>) .60, 1.00, 1.40, <u>1.80</u>	
8	3791.41	Si III(5)	0.50	(.00) .50	
9	3806.56	Si III(5)			
10	3813.39	Ti II(12)	1.19	(.05, .14, .24, <u>.33</u>) .90, 1.00, <u>1.19</u> , <u>1.29</u> , 1.38, 1.48	
11	3827.08	Fe II(153)	1.07	(.03, .09, .14) <u>1.00</u> , 1.06, 1.11, 1.17, 1.23, 1.28	
12	3853.66	Si II(1)	1.07	(.27, <u>.80</u>) .53, <u>1.07</u> , 1.60	
13	3856.02	Si II(1)	1.10	(.07, .20) <u>1.00</u> , 1.13, 1.27, 1.40	0.7
14	3862.59	Si II(1)	0.84	(.07) .73, <u>.87</u>	
15	3865.59	Cr II(167)	1.07	(.03, .09, .14) <u>1.00</u> , 1.06, 1.11, 1.17, 1.23, 1.28	0.7
16	3882.28	Ti II(34)	1.50	(.11, .33, .56, .78) .33, .56, .78, 1.00, 1.22, 1.44, 1.67, <u>1.89</u>	1.0
17	3900.55	Ti II(34)	1.11	(.00) 1.11	0.7
18	3913.46	Ti II(34)	0.89	(.00) 0.89	0.6
19	3932.01	Ti II(34)	1.50	(.11, .33, .56, .78) .33, .56, .78, 1.00, 1.22, 1.44, 1.67, <u>1.89</u>	
20	3935.94	Fe II(173)	1.06	(.02, .05, .08, 11) <u>1.00</u> , 1.03, 1.06, 1.10, 1.13, 1.16, 1.19, 1.22	0.7
21	3979.51	Cr II(183)	1.07	(.03, .09, .14) <u>1.00</u> , 1.06, 1.11, 1.17, 1.23, 1.28	
22	4012.50	Cr II(183)	0.90	(.03, .09) .77, <u>.83</u> , .89, <u>.94</u>	
23	4025.07	Fe III(53)	1.12	(.25, .50, .75, <u>1.00</u>) .25, .50, .75, <u>1.00</u> , <u>1.25</u> , 1.50, 1.75, 2.00	
24	4028.33	Ti II(87)	1.06	(.02, .05, .08, .11) <u>1.00</u> , 1.03, 1.06, 1.10, 1.13, 1.16, 1.19, 1.22	0.6
25	4038.03	Cr II(194)	1.04	(.01, .03, .05, .09) <u>1.00</u> , 1.02,, 1.16	
26	4048.83	Fe II(172)	1.14	(.00) 1.14	
27	4075.45	Si II[S]	1.10	(.07, .20) <u>1.00</u> , 1.13, 1.27, 1.40	0.7
28	4076.78	Si II[S]	0.84	(.07) .73, <u>.87</u>	
29	4077.71	Sr II(1)	1.17	(.33) <u>1.00</u> , 1.67	
30	4128.05	Si II(3)	0.90	(.03, .09) .77, <u>.83</u> , .89, <u>.94</u>	
31	4130.88	Si II(3)	1.03	(.17, .51, <u>.86</u>) .34, .69, <u>1.03</u> , 1.31, 1.71	
32	4139.37	Fe III(118)	1.84	(.17, .33, <u>.50</u>) 1.42, 1.58, <u>1.75</u> , <u>1.92</u> , 2.08, 2.25	1.1
33	4145.77	Cr II(162)	1.20	(.00), 1.20	0.7
34	4163.64	Ti II(105)	1.07	(.03, .09, .14) <u>1.00</u> , 1.06, 1.12, 1.16, 1.22, 1.28	0.7
35	4164.79	Fe III(118)	1.30	(.00, .15,, .60) <u>1.00</u> , 1.15,, 2.20	
36	4166.86	Fe III(118)	1.70	(.10, .20, .30, <u>.40</u>) 1.35, 1.45, 1.55, <u>1.65</u> , <u>1.75</u> , 1.85, 1.95, 2.05	
37	4171.90	Ti II(105)	0.90	(.03, .09) .77, <u>.83</u> , .89, <u>.94</u>	0.5
38	4173.45	Fe II(27)	1.48	(.11, .34, <u>.57</u>) 1.03, 1.26, <u>1.48</u> , 1.72, 1.94	0.7
39	4178.86	Fe II(28)	0.80	(.18, .54, .90) .35, .70, 1.06, 1.42, 1.78, 2.14	
40	4190.74	Si II [S]	1.10	(.07, .20) <u>1.00</u> , 1.13, 1.27, 1.40	
41	4198.13	Si II [S]	0.84	(.07) .73, .87	
42	4215.52	Sr II (1)	1.33	(.67) 1.33	0.6
43	4233.17	Fe II(27)	1.17	(.09, .26, .43) <u>1.00</u> , 1.17, 1.34, 1.52, 1.69	0.7
44	4242.38	Cr II(31)	1.17	(.05, .14, .24, .33) <u>1.00</u> , 1.10, 1.19, 1.29,, 1.67	0.6
45	4261.92	Cr II(31)	1.13	(.07, .20, .33) .91, 1.04, 1.17, 1.30, 1.43	0.7
46	4275.57	Cr II(31)	0.90	(.09, .26) .77, <u>.94</u> , 1.12, 1.29	
47	4284.21	Cr II(31)	0.50	(.20) .20, <u>.60</u>	
48	4287.89	Ti II(20)	1.50	(.20, .60) .60, 1.00, 1.40, <u>1.80</u>	0.9

TABLE 2 (CONT'D)

$\Delta\lambda_c$	Line No.	λ	El. (RMT) [†]	Z	Zeeman Pattern [‡]
0.7	*49	4290.22	Ti II(41)	1.10	(.18, .54) .83, 1.19, 1.55, 1.92
0.7	*50	4294.10	Ti II(20)	1.20	(.00) 1.20
0.8	*51	4300.05	Ti II(41)	1.22	(.09, .26, .43) <u>1.00</u> , 1.17, 1.34, 1.52, 1.68, 1.86
0.8	*52	4307.90	Ti II(41)	1.47	(.27, .80) .93, <u>1.47</u> , 2.00
0.8	*53	4312.86	Ti II(41)	1.48	(.11, .34, .57) 1.03, 1.26, <u>1.48</u> , 1.72, 1.94
0.8	*54	4314.98	Ti II(41)	1.33	(1.33) 1.33
	55	4351.76	Fe II(27)	1.10	(.18, .54) .83, 1.19, 1.55, 1.92
0.9	56	4354.36	Fe II(213)	1.43	(.00) 1.43
1.5	56a	4365.56	Fe III(4)	2.50	(.00) 2.50
0.6	*57	4367.66	Ti II(104)	1.06	(.02, .05, .08, .11) <u>1.00</u> , 1.03, 1.06, 1.10, 1.13, 1.16, 1.19, 1.22
1.1	57a	4382.31	Fe III(4)	1.83	(.00) 1.83
0.8	*58	4385.38	Fe II(27)	1.33	(1.33) 1.33
0.6	59	4386.86	Ti II(104)	0.93	(.02, .05, .08) 81, .84, .87, .90, .94, <u>.97</u>
0.7	60	4395.03	Ti II(19)	1.07	(.03, .09, .14) <u>1.00</u> , 1.06, 1.11, 1.17, 1.23, 1.28
0.8	*61	4399.77	Ti II(51)	1.40	(.02, .06) 1.31, 1.35, 1.39, <u>1.43</u>
0.6	62	4411.08	Ti II(115)	0.90	(.03, .09) .77, .83, .89, <u>.94</u>
1.0	*63	4419.59	Fe III(4)	1.67	(.00) 1.67
	64	4421.95	Ti II(93)	1.07	(.27, .80) .53, <u>1.07</u> , 1.60
0.9	*65	4430.95	Fe III(4)	1.50	(.00, .17, .33) <u>1.33</u> , 1.50, 1.67, 1.83, 2.00
0.6	66	4443.80	Ti II(19)	0.90	(.03, .09) .77, .83, .89, <u>.94</u>
0.6	*67	4450.49	Ti II(19)	1.03	(.17, .51, .86) .34, .69, <u>1.03</u> , 1.37, 1.71
	68	4464.46	Ti II(40)	0.53	(.93) <u>.13</u> , 1.73
0.6	69	4468.49	Ti II(31)	1.06	(.02, .05, .08, .11) <u>1.00</u> , 1.03, 1.06, 1.10, 1.13, 1.16, 1.19, 1.22
0.6	*70	4488.32	Ti II(115)	1.07	(.03, .09, .14) <u>1.00</u> , 1.06, 1.11, 1.17, 1.23, 1.28
	71	4491.40	Fe II(37)	0.40	(.00) .40
0.6	72	4501.27	Ti II(31)	0.93	(.02, .05, .08) .81, .84, .87, .90, .94, <u>.97</u>
	73	4508.28	Fe II(38)	0.50	(.20) .20, <u>.60</u>
0.7	74	4515.34	Fe II(37)	1.03	(.00) 1.03
0.9	75	4520.22	Fe II(37)	1.50	(.05, .14, .24, .33) <u>1.00</u> , 1.10, 1.19, 1.29, ..., 1.67
0.6	*76	4522.63	Fe II(38)	0.90	(.09, .26) <u>.77</u> , .94, 1.12, 1.29
	77	4529.46	Ti II(82)	1.01	(.10, .30, ..., .91) .20, .40, .61, .81, <u>1.01</u> , ..., 1.82
0.7	*78	4533.97	Ti II(50)	1.10	(.07, .20) <u>1.00</u> , 1.13, 1.27, 1.40
	79	4552.65	Si III(2)	1.25	(.00, .50) <u>1.00</u> , 1.50, 2.00
0.7	80	4555.89	Fe II(37)	1.24	(.00) 1.24
0.7	*81	4558.66	Cr II(44)	1.17	(.05, .14, .24, .33) <u>1.00</u> , 1.10, 1.19, 1.29, ..., 1.67
0.9	82	4563.76	Ti II(50)	0.83	(.07) .73, <u>.87</u>
1.1	*83	4567.87	Si III(2)	1.75	(.50) 1.50, 2.00
0.6	84	4571.97	Ti II(82)	0.95	(.01, .03, .05, .07) .84, .86, ..., <u>.98</u>
1.1	*85	4574.78	Si III(2)	2.00	(.00) 2.00
0.7	*86	4583.83	Fe II(38)	1.17	(.05, .14, .24, .33) <u>1.00</u> , 1.10, 1.19, 1.29, ..., 1.67
0.7	*87	4588.22	Cr II(44)	1.08	(.07, .20, .33) <u>.91</u> , 1.04, ..., 1.57
	88	4589.96	Ti II(50)	1.07	(.27, .80) .53, <u>1.07</u> , 1.60
	89	4592.09	Cr II(44)	1.20	(.17, .51, .86) .51, .86, <u>1.20</u> , 1.54, 1.89
	90	4618.83	Cr II(44)	0.90	(.09, .26) <u>.77</u> , .94, 1.12, 1.29
0.8	91	4629.34	Fe II(37)	1.33	(.00) 1.33
0.1	92	4634.11	Cr II(44)	0.50	(.20) .20, <u>.60</u>
	93	4635.33	Fe II(186)	1.07	(.03, .09, .14) <u>1.00</u> , 1.06, 1.11, 1.17, 1.23, 1.28

[†]An S in brackets indicates that the term values have been taken from Shenstone (1961).

[‡]The π components are in parentheses The most intense components in the π and σ groups are underlined

spectral type near B3 or B4. The strength of C II $\lambda 4267$ corresponds to type B8 while the He I lines are no stronger than those of a B9 star, but these anomalies are to be expected since Searle and Sargent (1964) have found that apparent underabundances of He and C are general characteristics of the Si-4200 class, of which HD 215441 is a member.

III. MEASUREMENTS OF THE ZEEMAN EFFECT

Spectrogram ECZ 5931 has been used to study the Zeeman effect in HD 215441 in detail. The displacements $\Delta\lambda_c$ between the σ_+ components in the sense right-circularly analyzed *minus* left-circularly analyzed are listed in Table 2; the quantity $\Delta\lambda_c$ is related to the observed shift $\Delta\lambda$ by

$$\Delta\lambda_c = \left(\frac{4500}{\lambda}\right)^2 \Delta\lambda. \quad (1)$$

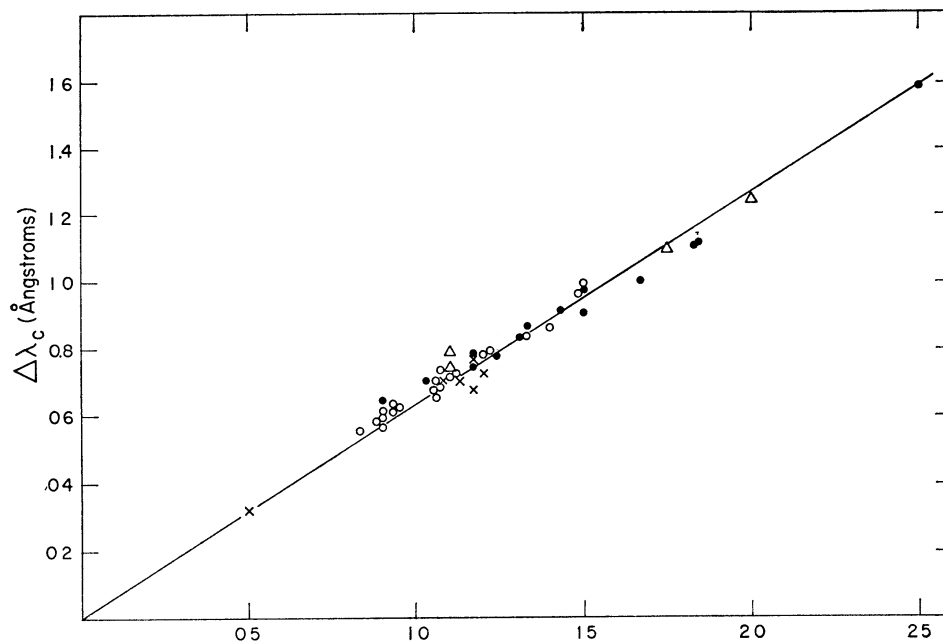


FIG. 2.—Correlation for ECZ 5931 between $\Delta\lambda_c$, the relative displacement of the σ_+ components, and z for lines of Fe II and Fe III (*filled circles*), Ti II (*open circles*), Cr II (*crosses*), and Si II and Si III (*triangles*). The least-squares line through the origin corresponds to a magnetic field of 33890 ± 170 gauss.

In Figure 2 we show a plot of $\Delta\lambda_c$ versus z . The z -values for LS coupling, also given in Table 2, were calculated with the aid of Kiess and Megger's (1928) tables. The displacements for all ions are well represented by a single straight line whose slope corresponds to a magnetic field of 33890 ± 170 gauss. The results show that in this star and at this particular phase the magnetic field affects all elements to the same degree and, incidentally, gives further evidence of the uniform results obtained by assuming that LS coupling prevails for the ions of the elements Si through Fe.

The lines whose Zeeman patterns were consistently resolved on 8 \AA mm^{-1} spectrograms are indicated by asterisks in column 1 of Table 2. In general, they are strong lines with large z -values or lines whose doublet patterns are resolved at the lower dispersion because of the weakness or absence of the undisplaced π component. Since the z -value for such lines cannot be calculated by application of Russell's rule (centroid of the σ group lies one-quarter of the way from the strongest to the weakest σ component),

empirical z -values were derived for these lines in the following way. Plots of Δs_c versus z shown in Figures 3 and 4 were made for each spectrogram by use of lines with calculable z -values, and least-squares slopes through the origin were computed for each. The measured Δs_c values for the doublets were then used to estimate z for each doublet. These are listed in Table 3. The mean z -values calculated from all plates, also given in Table 3, were then adopted for these lines which were included in the final least-squares solutions for the slopes and hence the magnetic fields that are listed in Table 1. The probable errors for fields derived from the 4 and 8 \AA mm^{-1} plates are typically 200 and 700 gauss, respectively.

IV. THE MAGNETIC VARIATION

A photometric period of 9^d.49 for HD 215441 was discovered by Jarzebowski (1960) in 1959. Stepien (1968) revised this value slightly by forcing Jarzebowski's and his own times of maximum light in 1967 to coincide. The resulting elements are:

$$\text{Light maximum} = \text{J.D. } 2436865.0 + 9.488 E. \quad (2)$$

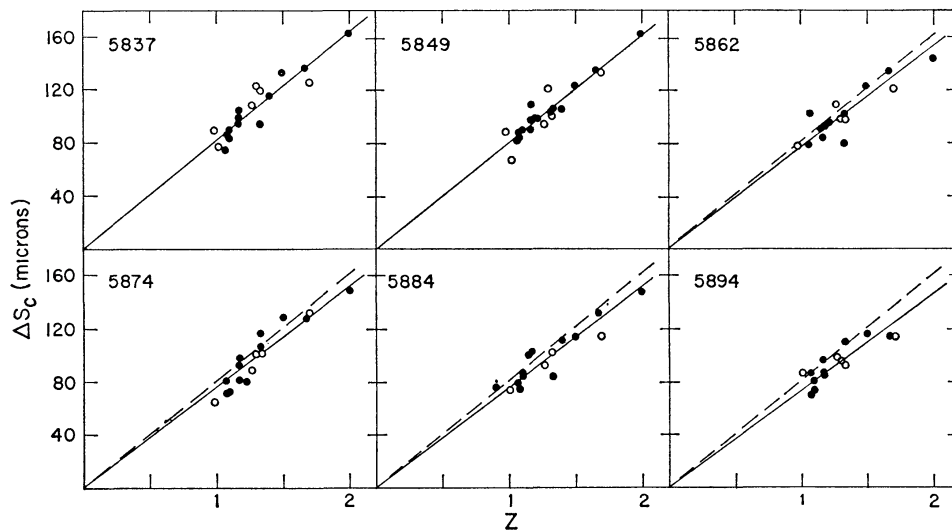


FIG. 3.—Correlation between Zeeman displacement Δs_c and z for the 8 \AA mm^{-1} spectrograms of HD 215441. The data plotted are those for the 8 \AA mm^{-1} line list indicated by asterisks in Table 2. Lines with empirical z -values taken from Table 3 are indicated by open circles. The least-squares line for ECZ 5837 is repeated as a dashed line for ECZ 5862, 5874, 5884, and 5894. The differences between the slopes of the dashed and solid lines in these cases constitute the evidence for a magnetic variation in HD 215441.

TABLE 3
EMPIRICAL z VALUES

LINE No.	λ	z		
		8 \AA mm^{-1}	4 \AA mm^{-1}	Adopted
38	4173 45	1.26	1.28	1.27
42	4215 52	0.96	1.06	1.01
52.	4307.90	1.39	1.22	1.30
53	4312 86	1.32	1.35	1.33
67	4450 49	1.02	0.95	0.98
83	4567 87	1.66	1.74	1.70

Phases calculated for the magnetic observations by means of these elements are given in Table 1. Plots of magnetic field versus phase calculated by means of these photometric elements indicate that the magnetic field does vary periodically and in phase with the light variation. This conclusion depends primarily on the 8 \AA mm^{-1} spectrograms which are the most numerous, but it is also supported by the four 4 \AA mm^{-1} plates. Comparison of the two series suggests that the field values from the 8 \AA mm^{-1} material are about 500 gauss larger than the relatively error-free 4 \AA mm^{-1} data. Since the Zeeman patterns are barely resolved on the 8 \AA mm^{-1} plates, we suspect that a bias operates which causes us to measure a line when grain fluctuations enhance the separation of the components but to reject a line when such fluctuations degrade the apparent resolution. If the systematic shift is attributed to this cause, then it is justifiable to remove it empirically by correcting the 8 \AA mm^{-1} by a constant downward shift so that the two sets coincide. If this relatively small correction of -500 gauss ($\sim 1 \mu$) is applied to the 8 \AA mm^{-1} data, we obtain the results shown in Figure 5. The measured field appears to

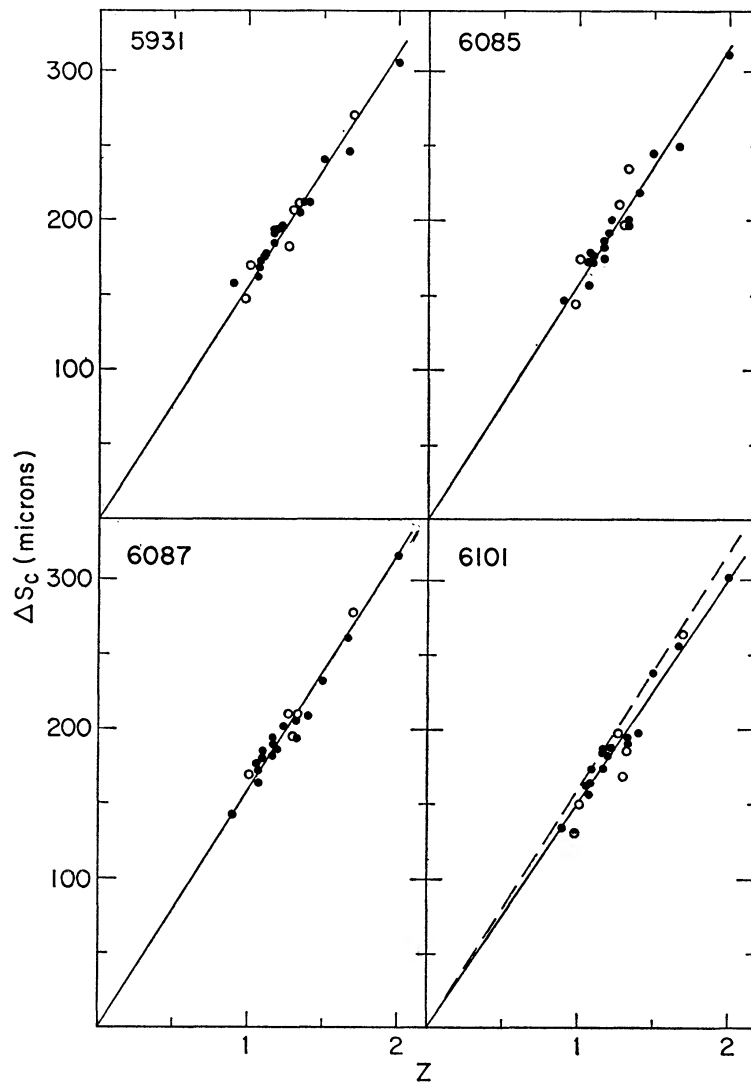


FIG. 4.—Correlations between Zeeman displacement Δs_c and z for the 4 \AA mm^{-1} spectrograms of HD 215441. Coding is as in Fig. 3. Slope of the least-squares line for ECZ 6087 is repeated as a dashed line in the diagram for ECZ 6101.

oscillate with a range of approximately 3000 gauss, a 10 percent variation, in phase with the light variation.

The light and magnetic variations are accompanied by a subtle kind of spectrum variability. The absorption-line spectrum is less distinct at magnetic minimum (phase 0.5) than at maximum (phase 0.0). This phenomenon, most noticeable for weak lines, is clearly visible when ECZ 5884 and 5894 are compared with ECZ 5837 and 5849. Babcock called attention to such variations and noted that the lines were strong on July 20, 1960, and weak on November 16, 1960. The phases on these dates according to equation (2) are 0.98 and 0.50, respectively. The radial velocity of HD 215441 appears to remain very nearly constant. The mean velocity from all the spectrograms is -5.5 ± 0.15 km sec $^{-1}$. The probable error of a single plate is about ± 0.5 km sec $^{-1}$.

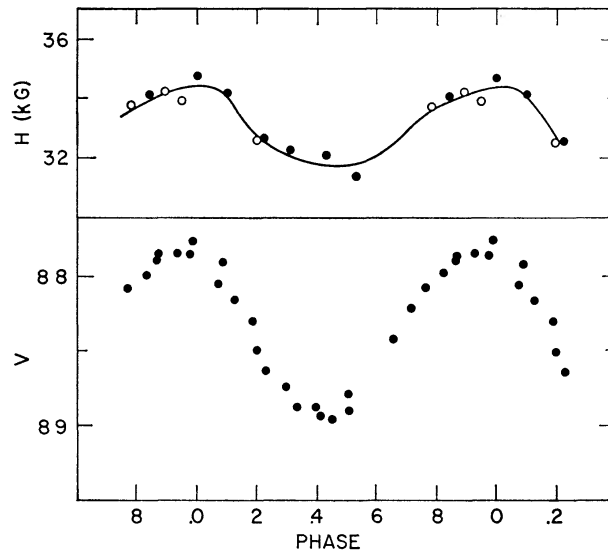


FIG. 5.—Variations of the magnetic field and visual light of HD 215441. Phases are calculated from equation (2) due to Stepien (1968). The photometry is also that of Stepien. Open and filled circles in the upper panel denote fields derived from 4 \AA mm^{-1} and 8 \AA mm^{-1} spectrograms, respectively. An arbitrary correction of -500 gauss has been applied to the latter data in this figure.

V. THE RESOLVED ZEEMAN COMPONENTS OF A STELLAR MAGNETIC DIPOLE FIELD

It is of some interest to determine the extent to which an oblique dipole rotator (Stibbs 1950; Deutsch 1954) can be made to represent the intensities and displacements of the resolved Zeeman line components of HD 215441. Previous studies have been concerned with the centroid of an unresolved triplet pattern. The result obtained by Schwarzschild (1950) for an inclined dipole is

$$H_e = \left(\frac{15 + u}{15 - 5u} \right) \frac{H_p}{4} \cos \alpha, \quad (3)$$

where H_p is the polar field strength and α is the angle between the line of sight and the dipole axis. In the present study magnetic fields have been inferred from the displacements of the σ components rather than the centroids of the triplet patterns, so that equation (3) does not apply. We calculate the intensities and displacements of the components of a normal Zeeman triplet formed by an inclined stellar dipole field in the notation of Schwarzschild (1950).

In a coordinate system (x, y, z) oriented so that the z -axis is parallel to the magnetic

axis of symmetry, the components of the magnetic vector at the surface of a star with unit radius have magnitudes

$$H_x = \frac{3}{2}H_p xz, \quad H_y = \frac{3}{2}H_p yz, \quad H_z = \frac{H_p}{2}(3z^2 - 1), \quad (4)$$

with

$$H = \frac{H_p}{2}(3z^2 + 1)^{1/2}, \quad (5)$$

where H_p is the polar field strength. Let the line of sight from the observer to the star lie in the (x, z) -plane. A second coordinate system (ξ, η, ζ) oriented so that the ζ -axis is parallel to the line of sight is related to the (x, y, z) coordinates by the transformation

$$\begin{aligned} x &= \zeta \sin \alpha + \xi \cos \alpha, \\ y &= \eta, \\ z &= \zeta \cos \alpha - \xi \sin \alpha. \end{aligned} \quad (6)$$

This transformation can then be used to obtain

$$\cos \gamma = \frac{H_\zeta}{H} = \frac{H_z \cos \alpha + H_x \sin \alpha}{H}, \quad (7)$$

or, after substitution and rearrangement,

$$\cos \gamma = \frac{(3\zeta^2 - 1) \cos \alpha - 3\xi\zeta \sin \alpha}{[3(\zeta \cos \alpha - \xi \sin \alpha)^2 + 1]^{1/2}}. \quad (8)$$

Let X be the displacement of a σ component from its field-free position in units of its displacement at the pole so that

$$X = \frac{1}{2}[3(\zeta \cos \alpha - \xi \sin \alpha)^2 + 1]^{1/2}. \quad (9)$$

Now the intensities of the Zeeman components as viewed through a circular analyzer are (Seares 1913)

$$i_{\sigma\pm} = \frac{1}{4}(1 \pm \cos \gamma)^2, \quad i_\pi = \frac{1}{2} \sin^2 \gamma. \quad (10)$$

If the usual limb-darkening law is employed,

$$I = 1 - u + u\zeta, \quad (11)$$

then the total intensities of the Zeeman components in integrated light may be written as

$$\mathfrak{I} = \frac{\int \int i I d\xi d\eta}{\int \int I d\xi d\eta}, \quad (12)$$

and the displacements of their centroids are given by

$$\langle X \rangle = \frac{\int \int X i I d\xi d\eta}{\int \int i I d\xi d\eta}. \quad (13)$$

We have integrated equations (12) and (13) numerically as follows. Loci of constant X defined by equation (9) were plotted on a disk of unit radius for $X = 0.55, 0.60, 0.70, 0.80, 0.90,$ and 0.95 as in Figure 6. Then the cosine of γ was calculated along the centers of the strips defined by adjacent pairs of these loci. The quantities $i_{\sigma+}, i_{\sigma-}, i_\pi,$ and I (for $u = 0.5$) were then calculated for small arbitrary area elements ΔA of these strips

by means of equations (8), (10), and (11). Summation of the products $iI\Delta A$ along the strips of constant X then gave the integrated intensity between X_i and X_{j+1} , which we write as

$$\mathfrak{I}(X)\Delta X = \frac{\sum iI\Delta A}{\sum I\Delta A} \quad (14)$$

In this way we obtained the Zeeman-broadening functions $\mathfrak{I}(X)$ of the σ components for inclinations of the dipole axis $\alpha = 0^\circ, 22^\circ.5, 45^\circ, 67^\circ.5,$ and 90° given in Table 4 and

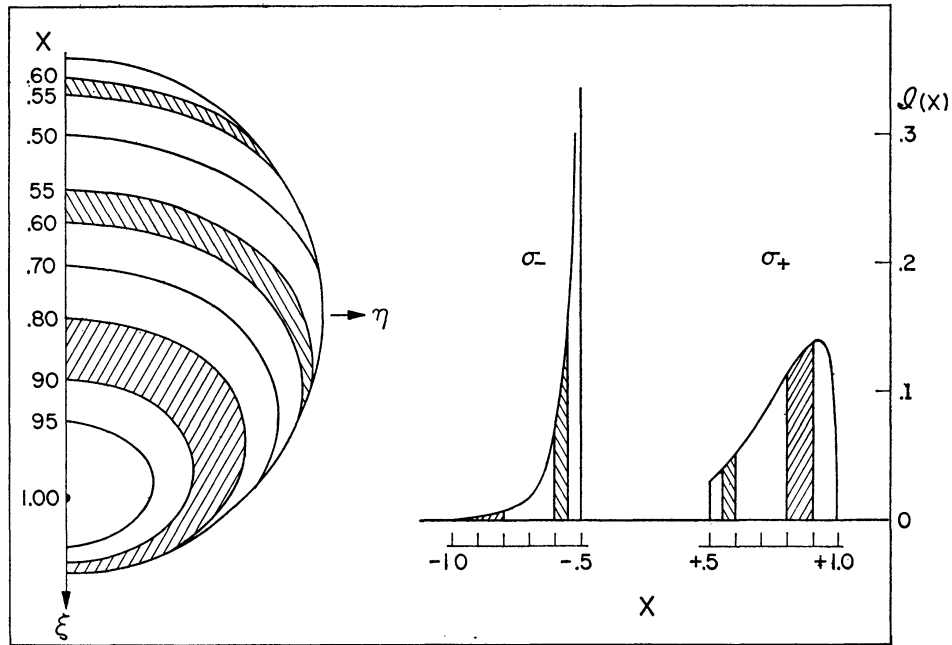


FIG. 6.—At left, loci of constant Zeeman displacement X are drawn on a stellar disk with a dipolar magnetic field, the axis of which is inclined 45° to the line of sight. The Zeeman-broadening functions $\mathfrak{I}(X)$ of the σ_+ and σ_- components that result from this configuration are shown at right. The contributions of the hatched areas of the stellar disk to the line profiles are indicated.

TABLE 4
PROFILES OF THE COMPONENTS OF A ZEEMAN TRIPLET
FORMED BY AN INCLINED STELLAR DIPOLE FIELD

X	$\mathfrak{I}(X)$									
	$\alpha = 0^\circ$		$\alpha = 22^\circ.5$		$\alpha = 45^\circ$		$\alpha = 67^\circ.5$		$\alpha = 90^\circ$	
	σ_+	σ_-	σ_+	σ_-	σ_+	σ_-	σ_+	σ_-	σ_+	σ_-
0.525	0 000	0 087	0 004	0 162	0 036	0 286	0 107	0 286	0 210	0 210
.575	005	078	016	069	046	088	082	104	106	106
.650	022	060	035	042	.060	.031	088	057	086	086
.750	068	035	080	026	.096	010	098	029	059	.059
.850	142	014	.133	.012	124	010	076	010	037	037
.925	218	002	.194	006	142	007	075	004	022	022
0 975	0 284	0 000	0 271	0 000	0 118	0 005	0 052	0 003	0 010	0 010

shown in Figure 7. If the visible magnetic pole is positive and the analyzer passes right-hand circularly polarized light, then the wavelength increases in the positive- X direction, and both the σ_+ and σ_- components have pronounced wings extending to shorter wavelengths. As the inclination α increases, the asymmetry of the σ_+ component reverses until, when $\alpha = 90^\circ$, the σ_+ and σ_- profiles are mirror images. Note that the Zeeman-broadening function for dipole geometry always lies in the interval $\frac{1}{2} \leq X \leq 1$. This stricture applies, of course, only to a non-rotating star. Comparison of the surfaces of constant Zeeman displacement in Figure 6 with those of constant Doppler displacement due to rotation about an arbitrary axis indicates that the calculation of rotational effects on the Zeeman-broadening function is a formidable one, and it is not attempted here.

The profiles of Figure 7 can be integrated immediately to give

$$\mathfrak{S} = \int \mathfrak{S}(X) dX, \quad \text{and} \quad \langle X \rangle = \frac{1}{\mathfrak{S}} \int X \mathfrak{S}(X) dX. \quad (15)$$

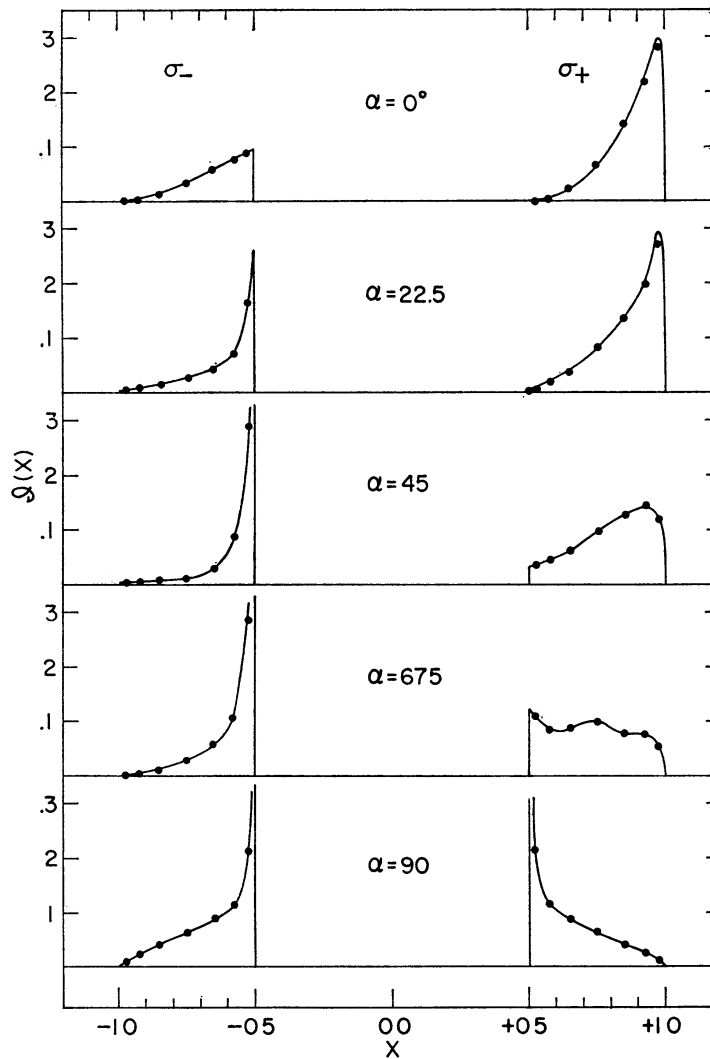


FIG. 7.—The broadening functions $\mathfrak{S}(X)$ for the σ_- and σ_+ components of a Zeeman triplet produced by inclined stellar dipole fields.

The results of these integrations, given in Table 5, are plotted versus α in Figure 8, *a* and *b*. The values of $\langle X \rangle$ for the σ_- component have been plotted with reversed sign. As a check on the calculations, we have computed values of H_e/H_p which should agree with equation (3). By the reasoning of Babcock (1947) we have

$$\frac{H_e}{H_p} = \frac{\langle X \rangle_{\sigma_+} \mathfrak{I}\sigma_+ - \langle X \rangle_{\sigma_-} \mathfrak{I}\sigma_-}{\mathfrak{I}\sigma_+ + \mathfrak{I}\sigma_- + \mathfrak{I}\pi}. \quad (16)$$

To allow for errors in the individual integrations, we use smoothed values taken from the freehand curves in Figure 8, *a* and *b*. The results, also given in Table 5 and shown

TABLE 5
INTENSITIES AND MEAN DISPLACEMENTS OF ZEEMAN COMPONENTS
FOR AN INCLINED STELLAR DIPOLE FIELD

	α (degrees)				
	0	22.5	45	67.5	90
\mathfrak{I} :					
σ_+	+0 485	+0 490	+0 450	+0 420	+0 358
π	+ .322	+ 300	+ 300	+0 285	+0 280
σ_-	+ 192	+ 198	+ 245	+0 295	+0 358
$\langle X \rangle$:					
σ_+	+ 88	+ 86	+ 80	+0 73	+0 65
π	00	.00	00	0 00	0 00
σ_-	- 65	- .61	- 58	-0 60	-0 65
H_e/H_p	307	.292	225	0 122	0 000
$0.31 \cos \alpha$.310	.286	.220	0 118	0 000
$\mathfrak{I}\pi/\mathfrak{I}\sigma_+$	64	64	66	0 72	0 78
$\mathfrak{I}\sigma_-/\mathfrak{I}\pi$	0 60	0 66	0 81	1 02	1 28

in Figure 8, *c*, are in satisfactory agreement with equation (3), which is also plotted for $u = 0.5$ as the curve in Figure 8, *c*.

With these results we are able to interpret the observed magnetic variation in terms of the oblique rotator, and in particular to estimate β , the angle between magnetic and rotation axes. Let r be the ratio of minimum to maximum values of $\cos \alpha$, as defined by Preston (1967). Then

$$\tan \beta = \left(\frac{1-r}{1+r} \right) \cot i, \quad (17)$$

where i is the angle between the rotation axis and the line of sight. The period (in days) and the equatorial rotational velocity (in kilometers per second) are related by

$$v_e = \frac{50.6 R}{P}, \quad (18)$$

where R is in units of solar radii. For $R = 2.5$ and $P = 9.45$, we have $v_e = 13$ km sec⁻¹. Babcock estimated $v_e \sin i \leq 4$ km sec⁻¹. Half-widths of resolved Zeeman components measured on intensity tracings of ECZ 5931, corrected by instrumental broadening, yield a similar estimate of $v_e \sin i \sim 5$ km sec⁻¹, so that $\sin i \sim 0.4$ or $i \sim 25^\circ$.

The field variation of Figure 5 implies a 10 percent variation in $\langle X \rangle_{\sigma_+}$. Since $\mathfrak{S}_{\sigma_+}/\mathfrak{S}_{\sigma_-} > 1$ on all our spectrograms, we infer that $\alpha < 60^\circ$ throughout the cycle. If we take $(\cos \alpha)_{\max} = 1.0$, then a variation of $\langle X \rangle_{\sigma_+}$ from 0.88 to 0.79 leads to $(\cos \alpha)_{\min} = 0.7$ or $r = 0.7$. These values of i and r in equation (17) then lead to $\beta \sim 20^\circ$.

If, on the other hand, we choose $R = 5$ as more appropriate for a main-sequence star of spectral type B3, then $i \sim 12^\circ$ and $\beta \sim 40^\circ$. Thus HD 215441, treated as an oblique dipole rotator, has a magnetic axis less inclined to its rotation axis than the majority of periodic variables (Preston 1967). Further elaboration of this point is not warranted, in view of a discrepancy described below.

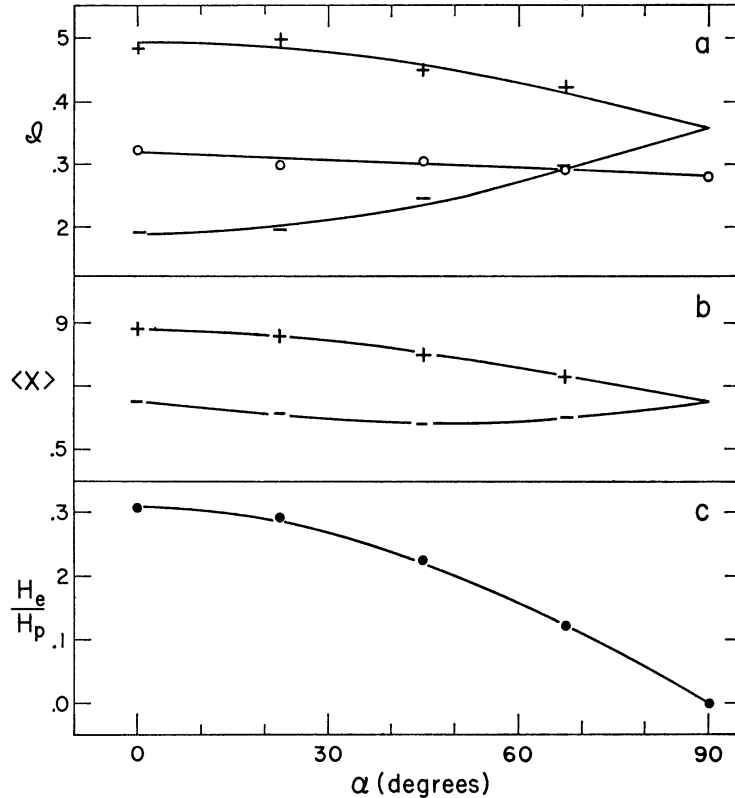


FIG. 8.—The variations of (a) the total intensities \mathfrak{S} and (b) centroid displacements $\langle X \rangle$ of the components of a Zeeman triplet with α , the inclination of the dipole axis to the line of sight. The calculations for the σ_+ , π , and σ_- components are indicated by the symbols +, o, and -. Freehand curves have been drawn through the model calculations. In the bottom panel the quantity H_e/H_p defined by equation (16) is compared with the cosine law of equation (3).

VI. THE GEOMETRY OF THE SURFACE FIELD INFERRED FROM THE ZEEMAN PROFILES

Because of the limited resolution of the Zeeman components in HD 215441, due to a combination of Doppler and instrumental broadening, we cannot compare the observed line shapes with those of the dipole calculations. Therefore, we restrict our attention to the total intensities \mathfrak{S} and the mean displacements $\langle X \rangle$. We have measured the equivalent widths W_λ for the σ_+ , σ_- , and π components of the twelve best triplets on $\lambda\lambda 4400$ – 4600 . For each line we then form the equivalent-width ratios π/σ_+ and σ_-/π given in Table 6 and plot the mean values of these ratios in Figure 9, where they can be compared with the calculations for the family of inclined dipoles. The agreement is not satisfac-

TABLE 6
EQUIVALENT WIDTHS AND η -RATIOS FOR SELECTED LINES
ON PLATE ECZ 5931 OF HD 215441

LINE No.	$W_\lambda(\text{m}\text{\AA})$			$W_\lambda(\sigma_-)/W_\lambda(\pi)$	$W_\lambda(\pi)/W_\lambda(\sigma_+)$	$\eta(\sigma_-)/\eta(\pi)$			$\eta(\pi)/\eta(\sigma_+)$		
	σ_-	π	σ_+			$v_D=2$ km sec $^{-1}$	$v_D=3$ km sec $^{-1}$	$v_D=4$ km sec $^{-1}$	$v_D=2$ km sec $^{-1}$	$v_D=3$ km sec $^{-1}$	$v_D=4$ km sec $^{-1}$
59...	41	73	84	0.56	0.87	0.19	0.32	0.39	0.54	0.65	0.71
62...	32	58	70	.55	.83	.35	.49	.54	.28	.43	.47
66	58	97	101	.60	.96	.15	.26	.34	.91	.93	.93
69	64	106	114	.60	.93	.16	.26	.33	.63	.69	.83
72	54	64	104	.84	.62	.58	.84	.71	.16	.26	.36
74	48	76	90	.63	.84	.23	.38	.42	.48	.59	.68
78	74	132	138	.56	.96	.02	.06	.10	.78	.83	.85
81	79	140	169	.56	.83	.08	.13	.21	.56	.42	.50
84	64	106	112	.60	.95	.14	.25	.33	.81	.81	.87
85	54	88	91	.61	.97	.17	.30	.36	.89	.93	.95
86...	87	117	148	.74	.79	.26	.33	.46	.36	.32	.47
87...	78	126	173	0.62	0.73	0.13	0.20	0.30	0.32	0.23	0.31
Avg.....	0.62	0.86	0.21	0.32	0.37	0.56	0.60	0.66

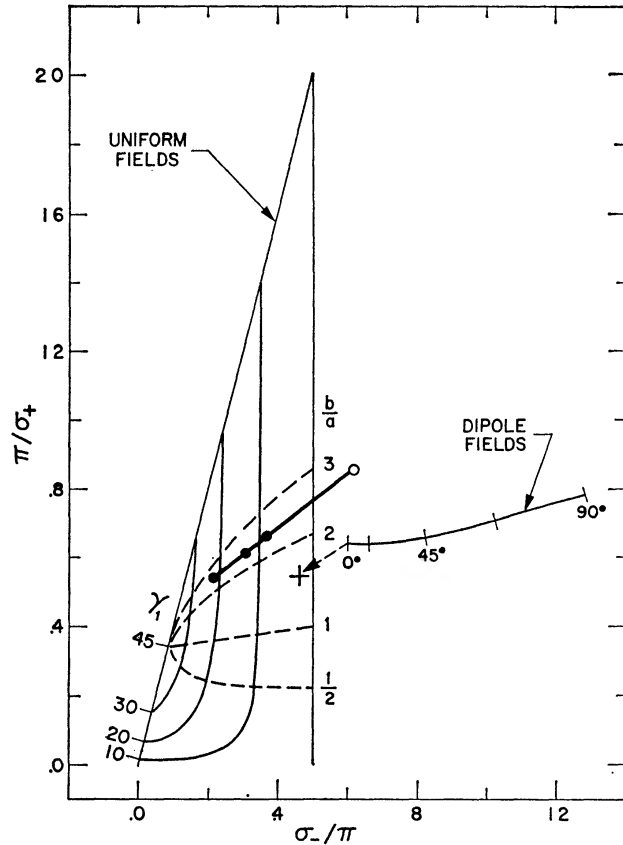


FIG. 9.—Comparison of the observed intensity ratios $\mathfrak{I}_\pi/\mathfrak{I}_{\sigma_+}$ and $\mathfrak{I}_{\sigma_-}/\mathfrak{I}_\pi$ with those calculated for inclined dipoles (Table 5), for uniform inclined fields (eq. 19), and for the arbitrary geometries that lead to equation (20). A plus sign indicates the position of the dipole model with the extreme limb-darkening coefficient $u = 1$. The equivalent ratios derived from ECZ 5931 are plotted as an open circle. The η -ratios for Doppler parameters of 4, 3, and 2 km sec $^{-1}$ are plotted as filled circles along a line extending down and to the left from the open circle.

tory. We expect that there is a curve-of-growth effect, since the calculated ratios apply to weak lines while the σ_+ components typically have equivalent widths of the order of 0.1 Å. Such values of W_λ place them on the transition portion of the curve of growth for any reasonable Doppler parameter. To take this effect into account, we have used Wrubel (1949) M.E. curves of growth for $B_0/B_1 = \frac{4}{3}$ and for Doppler parameters of $v_D = 4, 3,$ and 2 km sec^{-1} . At spectral type B4 the Doppler parameter due to thermal motions alone is about 2 km sec^{-1} . We read in W_λ values and read out η -values whose ratios, also given in Table 6, should be comparable to the theoretical values based on equation (10). As expected, the corrected points lie along a line that extends down and to the left. The fit does not improve; in fact, it appears to be poorer. However, the corrected position of the star in the $[(\pi/\sigma_+)(\sigma_-/\pi)]$ -plane better indicates the reason for the discrepancy; the π/σ_+ values are in reasonable agreement with the dipole calculations, so it appears that the stellar σ_- component is weaker than that expected for dipole geometry. Two points should be made with respect to this conclusion. First, any error in the instrumental phase-shift compensation will act to contaminate the right- and left-circularly analyzed spectra mutually and thus make the observed σ_- components *stronger* than the true stellar components. Second, we have limited this discussion to twelve lines principally because of the difficulty in finding measurable σ_- components; i.e., if anything, our results are biased toward large σ_- values due to plate grain fluctuations and unrecognized blending. Therefore, we do not believe that the above discrepancy is likely to be due to errors of observation or data reduction. The σ_- component of a dipole viewed at $\alpha = 0$ is formed mostly near the stellar limb. Therefore, a reduction in the limb contribution to the integrated light might be expected to move the theoretical (σ_-/π) -ratio nearer to the observed value. Accordingly, we have calculated the intensities for a dipole with $\alpha = 0$ for the severe limb-darkening coefficient $u = 1$. The result, plotted as a plus (+) sign in Figure 9, indicates that no ordinary distribution of surface brightness can improve the fit significantly. This conclusion also resulted from integrations in which central, circular regions of the disk were arbitrarily brightened by factors of 2 and 3. *Therefore, we are led to the important, if not unexpected, result that the magnetic field of HD 215441 is not dipolar.*

Additional support for this conclusion may be found in the observed value of $\langle X \rangle_{\sigma_-} / \langle X \rangle_{\sigma_+} = 0.93$ derived from thirteen triplets for which displacements of the σ_- components can be measured on ECZ 5931. From Figures 7 and 8 it is readily seen that so long as $\mathfrak{J}_{\sigma_-} / \mathfrak{J}_{\sigma_+}$ is substantially less than 1, as is the observed ratio, then $\langle X \rangle_{\sigma_-} / \langle X \rangle_{\sigma_+}$ is also substantially less than 1. For $\alpha \lesssim 50^\circ$ the value for dipoles is approximately 0.7. This implies that the σ_- and σ_+ components in HD 215441 are formed in regions of more nearly equal field strengths than is the case for a dipole.

We next consider how well the observed ratios compare with those for a uniform magnetic field. In this case we have, from equations (10),

$$\frac{\pi}{\sigma_+} = 2 \left(\frac{1 - \cos \gamma}{1 + \cos \gamma} \right), \quad \text{and} \quad \frac{\sigma_-}{\pi} = \frac{1}{2} \left(\frac{1 - \cos \gamma}{1 + \cos \gamma} \right). \quad (19)$$

As γ varies from 0° through 90° , these equations generate the straight line of slope 4 shown in Figure 9. The fit for $\gamma = 50^\circ$ or 60° is no worse than that for a dipole with $\alpha = 0$. We may summarize the above two comparisons as follows: (1) The magnetic geometry of HD 215441 is more complicated than that of a uniform field; (2) The observed ratios π/σ_+ and σ_-/π indicate the presence of a transverse field that is more dominant and a negative field that is less dominant than those presented by a dipole.

An infinite number of arbitrary geometries can be considered, but it is of some interest to see how we might account for the observed location of HD 215441 in Figure 9 by a geometry that conforms to the conclusions of the preceding paragraph. Accordingly, consider a family of stellar disks on which fractional areas a and b possess uniform but mutually perpendicular magnetic fields that are inclined to the line of sight at angles

γ_1 and $\gamma_2 = 90^\circ - \gamma_1$, respectively. The resultant intensities are thus linear combinations of equations (10):

$$i = ai(\gamma_1) + bi(\gamma_2). \quad (20)$$

Loci of such families obtained from equations (10) and (20) are plotted in Figure 9 for $\gamma_1 = 0^\circ, 10^\circ, 20^\circ$, and 30° . Lines of constant b/a are also indicated by dashed lines. The loci terminate on the locus for uniform inclined fields when $a = 0, b = 1$, and when $a = 1, b = 0$. It is possible to reproduce the observed π/σ_+ and σ_-/π ratios if γ is roughly 10° or 20° over some 30 percent of the disk and 70° or 80° over the remainder. Such an artificial model might be regarded as an approximation to a distorted dipole such as that shown in Figure 10, for which the magnetic vector remains largely radial down to colatitudes $\sim 80^\circ$. Such a geometry bears some resemblance to the class of distorted dipoles proposed recently by Böhm-Vitense (1967) to explain the anharmonic field variations of the periodic magnetic stars.

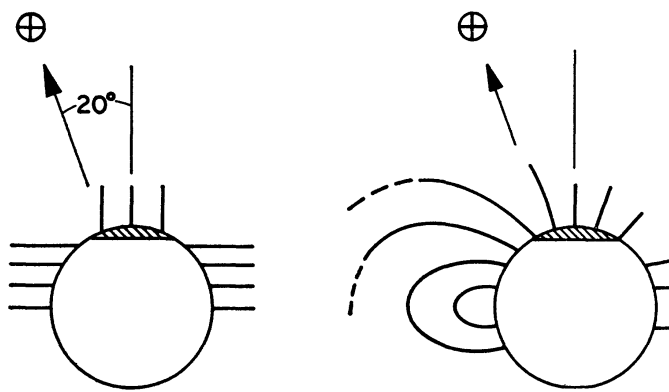


FIG. 10.—Schematic picture of the way in which the arbitrary geometry of equation (20) might approximate a divergence-free axisymmetric field.

Additional information may be gained from a study of the variations of the π/σ_+ and σ_-/π ratios during the course of the 9^d5 period, should such variations exist. Unfortunately, the small number of high-dispersion spectrograms now available and their poor distribution in phase do not permit such an investigation at present.

A portion of this research was supported by a grant from the National Science Foundation.

REFERENCES

- Babcock, H. W. 1947, *Ap. J.*, **105**, 105.
 ———. 1960, *ibid.*, **132**, 521.
 Böhm-Vitense, E. 1967, *Magnetism and the Cosmos* (New York: American Elsevier Publishing Co.), p. 179.
 Cameron, R. C. 1967, in *The Magnetic and Related Stars*, ed. R. C. Cameron (Baltimore: Mono Book Corp.), p. 471.
 Deutsch, A. J. 1954, in *I.A.U. Transactions*, **8**, 801.
 Jarzembowski, T. 1960, *Acta Astr.*, **10**, 119.
 Johnson, H. L. 1963, in *Basic Astronomical Data*, ed. K. Aa. Strand (Chicago: University of Chicago Press), p. 204.
 Kiess, C., and Meggers, W. 1928, *J. Res. N.B.S.*, **1**, 641.
 Osawa, K. 1965, *Ann. Tokyo Astr. Obs.*, **9**, 123.
 Preston, G. W. 1967, *Ap. J.*, **150**, 547.
 Schwarzschild, M. 1950, *Ap. J.*, **112**, 222.
 Seares, F. H. 1913, *Ap. J.*, **38**, 99.
 Searle, L., and Sargent, W. L. W. 1964, *Ap. J.*, **139**, 793.
 Shenstone, A. G. 1961, *Proc. R. Soc. London, A*, **261**, 153.
 Stepien, K. 1968, *Ap. J.*, **154**, 945.
 Stibbs, D.W.N. 1950, *M.N.R.A.S.*, **110**, 395.
 Underhill, A. 1957, *Pub. Dom. Ap. Obs.*, **10**, 357.
 Wrubel, M. 1949, *Ap. J.*, **109**, 71.